Journal of Structural Geology 32 (2010) 1466–1475

Contents lists available at ScienceDirect

Journal of Structural Geology

journal homepage: www.elsevier.com/locate/jsg

Insights into fold growth using fold-related joint patterns and mechanical stratigraphy

Heather M. Savage [a,*], J. Ryan Shackleton [b], Michele L. Cooke [b], Jeffrey J. Riedel [c]

[a] Lamont-Doherty Earth Observatory, Columbia University, Palisades, NY 10964, USA
[b] University of Massachusetts, Amherst, 611 North Pleasant St., Amherst, MA 01003 9297, USA
[c] 2907 Secor Avenue, Bozeman, MT 59715, USA

ARTICLE INFO

Article history:
Received 5 April 2010
Received in revised form
30 August 2010
Accepted 10 September 2010
Available online 17 September 2010

Keywords:
Sheep Mountain Anticline
Joint pattern
Mechanical stratigraphy
Plate bending

ABSTRACT

Despite how common folds are as structural features, along-strike fold propagation has proven elusive to document. However, if a fold grows laterally along its axis, early-formed fold-related joints may differ significantly in orientation from joints that form later. In this paper, we integrate mechanical stratigraphy with joint pattern analysis to determine relative timing of jointing. Additionally, we demonstrate that joint patterns can be related to stresses on both the top and bottom of the bed during flexure.

We present joint data from eight sedimentary beds on the fold terminus at Sheep Mountain Anticline, Wyoming, USA. The joint patterns around the terminus show two distinct patterns: joints in six of the beds show a radial pattern around the terminus whereas joint patterns in the two remaining beds differ from proximal units, despite being in the same structural position. Fracture resistance calculations confirm that the beds with mis-oriented fractures are less resistant to fracturing than other units in the study, and therefore would have fractured earlier in fold growth history. We present a plate bending model that illustrates potential joint patterns around a plunging fold nose from stresses along both the top and bottom of the bed. The joint strike predictions for the area in front of the inflection line on the fold nose match the orientations in our less resistant beds, which are now positioned behind the inflection line, suggesting that the fold grew laterally. The combined analysis of fracture pattern and mechanical stratigraphy provides a new way to investigate fold evolution.

1. Introduction

Folds are ubiquitous deformational structures, found in every tectonic setting, with economic impacts in both oil exploration and mining. Understanding the formation and growth of these structures will illuminate how progressive deformation is achieved, however direct observations of active folding are elusive. Active folding is assumed to be largely aseismic (Scholz, 2002), with some notable exceptions like the 1983 Coalinga earthquake (Stein and King, 1984), and GPS velocities attribute 100% of the observed deformation to fault slip. Nevertheless the omnipresence of folding within all deformational settings speaks to the role that this inelastic process must play in accommodating deformation during or between earthquakes.

Past growth of folds along their strike has been observed in the field through quartz deformation lamellae (e.g. Pavlis and Bruhn, 1988) as well as through geomorphic indicators (e.g. Jackson et al., 1996; Keller et al., 1999). Fischer and Wilkerson (2000) used kinematic models to demonstrate how fold-related jointing may record fold growth. The key region for unraveling the evolution of folding is at fold terminations where material is incorporated into the fold structure. These inherently three-dimensional regions must be carefully investigated with attention to temporal and spatial variations in fold shape as well as variations in stratigraphy. Here we further explore the relationship between fold growth and joint orientation, by considering the mechanical properties of different layers to provide a relative timescale of fracturing at Sheep Mountain Anticline, WY, USA. Furthermore, we consider stresses on the bottom as well as the top of a folded layer and compare these patterns to observed joint patterns.

Natural fractures are extremely common in folded sedimentary strata (e.g. Nelson, 1985). When bending stresses dominate, fold-related joints initiate along the outer arc of the fold where tangential longitudinal stresses are effectively tensile (e.g. Price and Cosgrove, 1990; Fig. 1A). These joints develop perpendicular to the direction of maximum curvature, which produces fractures that form a radial fanning pattern in map view around fold terminations

* Corresponding author.
E-mail address: hsavage@ldeo.columbia.edu (H.M. Savage).

0191-8141/$ – see front matter © 2010 Elsevier Ltd. All rights reserved.
doi:10.1016/j.jsg.2010.09.004

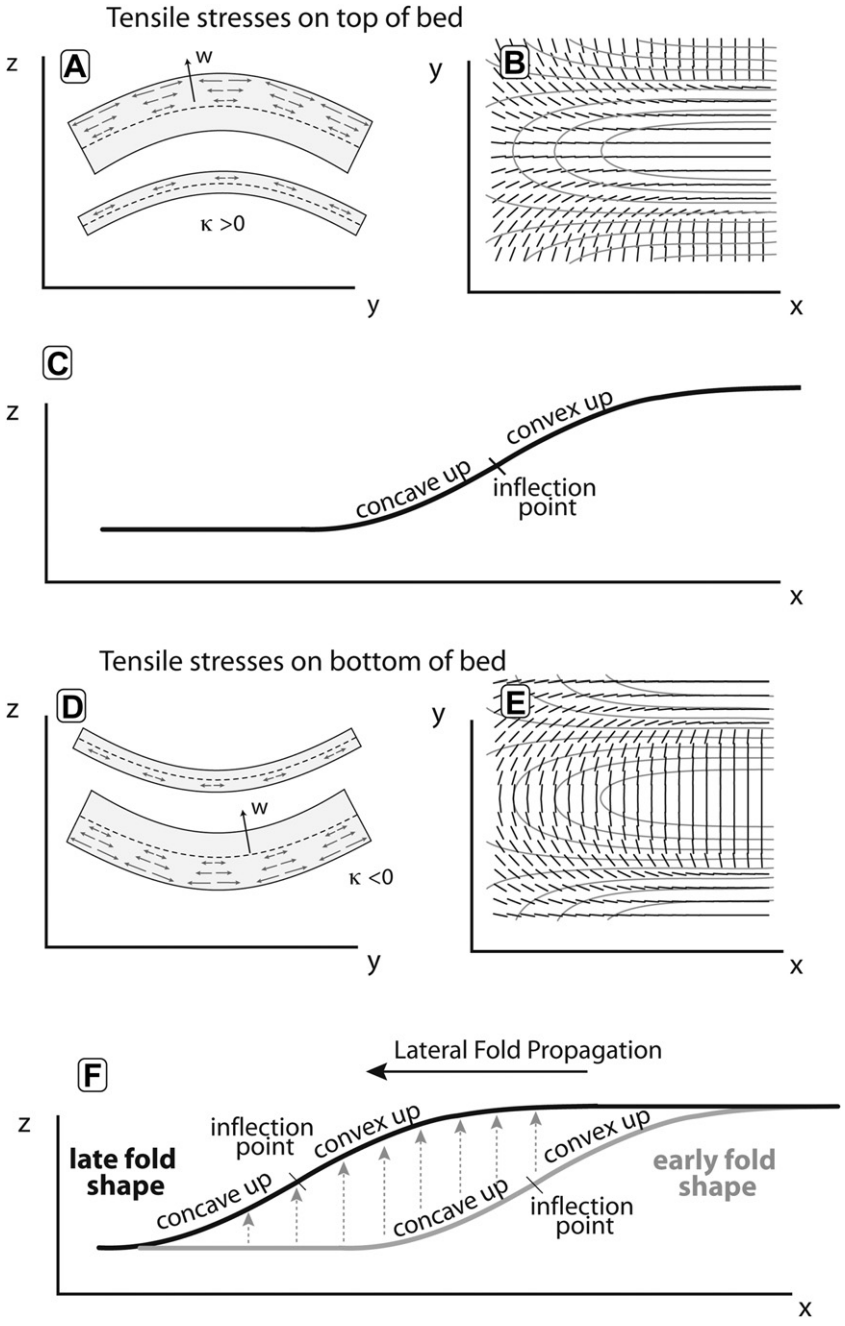

Fig. 1. A) Cross-section of a convex upwards fold. Tangential longitudinal stresses are greater for thicker beds and are maximum at the upper bed surface. B) Map view of plunging fold termination (gray structure contours) with joint strike orientation (black dashes) as predicted by numerical plate bending models from the maximum curvature directions on the top of the bed. C) Cross-section along the fold axis showing the inflection point in the profile where the curvature is zero. D) Cross-section of a convex downward fold. Tangential longitudinal stresses are maximum on the lower surface of the folded bed. E) Map view of plunging fold termination (gray structure contours) with joint strike orientation (black dashes) as predicted by numerical plate bending models from maximum curvature directions on the base of the bed. F) Cross-section along the fold axis showing early and later fold profiles. The gray dashed arrows show potential displacement paths of the bed during lateral fold propagation. Units that are in front of the inflection point early in folding may reside behind the inflection point later in folding. Consequently, joints that develop in front of the inflection point may reflect the former concave upward shape of this portion of the early fold.

of doubly-plunging anticlines (e.g. Fischer and Wilkerson, 2000; Fig. 1B). However, many studies document fold-related joint orientations that are uncorrelated with the direction of maximum curvature (e.g. Cruikshank et al., 1991; Engelder et al., 1997; Hennings et al., 2000). Explanations for these uncorrelated cases range from joints forming at some time other than folding, or by some mechanism other than outer arc stretching.

Another possible explanation for anomalous joint patterns in folds is the complexity in stress fields at fold terminations, due to the change in concavity at the inflection line across the fold nose (Fig. 1C). Beds on the anticline behind the inflection line, where the fold is convex up, will have a fracture pattern related to the stresses on the top of the layer. However, beds in front of the inflection line, where the fold is concave up, will have joint patterns related to the stresses on the bottom of the layer (Fig. 1D and E). Although tangential longitudinal normal stresses, or fiber stresses, exist on both the top and bottom surfaces of the bed, joints will initiate at the surface with greater effective tensile stress and propagate through

the thickness of the bed. Consequently, the joint pattern recorded reflects whether stresses were more effectively tensile on the top or bottom surface of the folded bed. Unlike most studies that only consider the stresses at the top surface during folding, we present a more comprehensive perspective that sheds light on apparently chaotic joint patterns by considering stresses on both the top and bottom of a folded layer that is jointing in response to tangential longitudinal stresses.

A second complexity to consider is lateral fault propagation, which changes the shape of associated folds, as well as maximum curvature directions, stresses, and joint orientations (Fischer and Wilkerson, 2000; Fig. 1F). For instance, the fractures that form in the concave up part of the fold could later be translated to a structural position where the fold is concave down and thus the earliest formed fractures will not reflect observed fold curvature.

Distinguishing fractures associated with multiple episodes of folding is complicated because joint terminations only record fracture timing with respect to other fractures and not specific folding episodes. However, the mechanical stratigraphy of the fractured units can provide additional information on fracture timing because beds with differing mechanical properties and thickness may fracture at different stages of fold evolution. Within a thin flexed layer, the tangential longitudinal stresses (σ_{TL} or fiber stresses) responsible for jointing are related to the layer curvature, κ, (Turcotte and Schubert, 2002) as

$$\sigma_{TL} = \frac{E}{(1-\nu^2)} wk \tag{1}$$

where E and ν are the elastic stiffness and Poisson's ratio of the material respectively and w is position relative to the neutral surface (Fig. 1A). In this formulation, positive curvature is convex upwards. For convex upwards folds tensile stresses arise for $w > 0$ and for convex downwards folds, tensile stresses arise for $w < 0$. Joints are expected to initiate where the σ_{TL} is most tensile; the maximum tangential longitudinal stress, σ_{TL}^{surf}, occurs at the top and bottom surfaces of the layer of thickness, H, where $|w| = H/2$.

$$\sigma_{TL}^{surf} = \pm\frac{EH}{2(1-\nu^2)}\kappa \quad \text{for } \kappa^{+/-} \tag{2}$$

Thicker and stiffer layers have greater tensile stress on the bed surfaces than thinner and softer layers within the same structural position. Joints will develop when σ_{TL}^{surf} meets the tensile strength of the bed, T. For a given structural position the curvature will be equal for all beds but the thickness, elastic properties and tensile strength might all differ so that fracturing should not be synchronous in all beds. We term the critical curvature for the development of joints in a layer the fracture resistance, F_r.

$$F_r = \frac{2T(1-\nu^2)}{EH} \tag{3}$$

Beds that have greater tensile strength and are thinner will have greater fracture resistance than thicker beds with lower tensile strength.

To investigate the effects of mechanical stratigraphy, plate bending and fold growth on fracture pattern, we document the earliest joint sets in several beds around the northern nose of Sheep Mountain Anticline, Bighorn Basin, Wyoming, USA (Fig. 2). The relative fracture timing of individual beds is predicted by using the thickness and material properties of each unit to estimate the

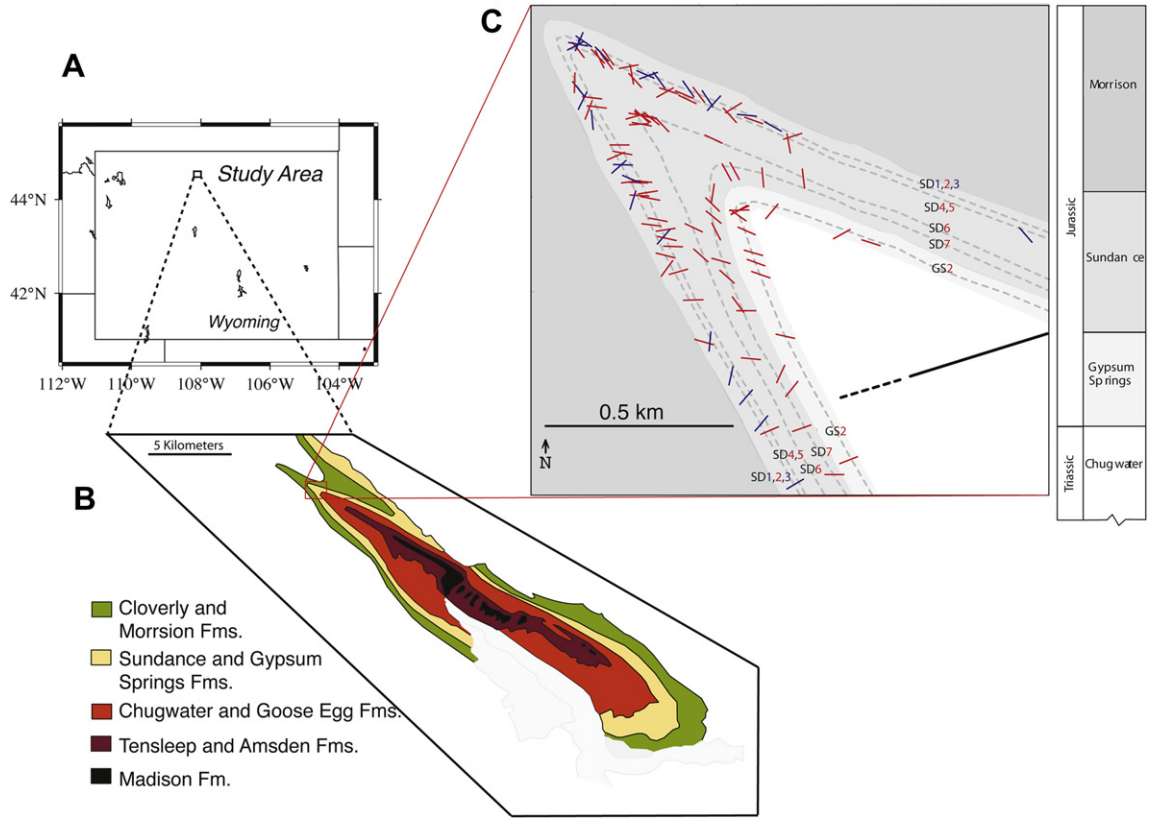

Fig. 2. A) Map of Wyoming, USA, showing the location of the field site. B) A simplified geologic map of Sheep Mountain Anticline (modified from Green and Drouillard, 1994). C) Earliest joint orientations measured around the nose of Sheep Mountain Anticline in the Sundance and Gypsum Springs Formations. All joint orientations have been rotated by restoring the bed dip to horizontal. The joints shown in red represent beds that generally show a radial fanning pattern around the nose of the fold. Joints shown in blue deviate from this pattern. The dashed gray line approximates the bed strike for several units around the fold, which are labeled.

fracture resistance. We use plate bending theory to predict the earliest formed joints at either the top or bottom of different layers of an anticline propagating laterally along its axis. Finally, we compare joints observed at Sheep Mountain Anticline to joint patterns from theoretically-derived fold shapes that incorporate lateral fold propagation to determine the structural position in which the least resistant beds could have fractured.

2. Sheep Mountain Anticline, WY

Sheep Mountain is a doubly plunging anticline with excellent exposure that has been the subject of several previous papers (Harris et al., 1960; Johnson et al., 1968; Hennier and Spang, 1983; Forster et al., 1996; Savage and Cooke, 2004; Stanton and Erslev, 2004; Bellahsen et al., 2006a,b; Allwardt et al., 2007; Amrouch et al., 2010). Like other structures in the Bighorn Basin, this NW–SE trending fold formed during the Laramide Orogeny due to slip along underlying, southwest-dipping basement reverse faults (Hennier and Spang, 1983; Stanton and Erslev, 2004). Early fracture studies at Sheep Mountain focused on the orientation of fractures in different structural positions along the fold and interpreted fractures oblique to present day bed strike as shear fractures (Harris et al., 1960; Johnson et al., 1968). More recent investigation reveals that many of the oblique to bed strike fractures are joints rather than shear fractures (e.g. Bellahsen et al., 2006a,b). Bellahsen et al. (2006a) used relative ages and commonality of joint sets to determine the timing of initiation in relation to fold growth. Allwardt et al. (2007) found that present day curvature on the outcrop scale correlates with variation in joint orientation but not intensity. Most recently, data on jointing and small faults were combined with calcite twinning analysis to determine the full stress history of Sheep Mountain (Amrouch et al., 2010).

2.1. Field observations of jointing

We present joint orientation data from several continuously exposed competent beds within the Jurassic Sundance and Gypsum Springs Formations (Fig. 2C). Each competent bed is bounded by less competent shale units. The thick shale of the Chugwater Formation lies below the Gypsum Springs Formation and above the upper tip of the fault that cores the fold. Fault–related stresses are expected to dissipate with significant bedding plane slip among the layers (e.g. Roering et al., 1997; Shackleton and Cooke, 2007). We observe abundant internal deformation, such as small faults, within the relatively low strength Chugwater Formation and therefore assume that stresses within overlying beds reflect primarily the flexural process.

We limited our study to the northwestern end of the fold because of poor exposure in the southeastern end. Although measurements were taken around the entire northwestern terminus, we restrict our study here to the more systematic joints on the southwest limb. The proximity of the northeast limb to the adjacent syncline may be responsible for the more chaotic joint pattern on that side of the fold. Fig. 2 documents the earliest joint sets at each sample location. Measurements were taken approximately 30 m apart when exposure was continuous, and at every large outcrop when exposure was less continuous. Joint sets were delineated as well-defined, repeating joint orientations that were pervasive throughout the outcrop (Fig. 3). We measured several individual joints in each set to ensure that joints were indeed parallel to subparallel. Although multiple joint sets were measured at each station, here we focus on the earliest formed set. Relative age was inferred from abutting relationships. The formation of the earliest joint set is not impacted by the presence of previously formed joints. Consequently, the earliest joints may reveal early fold shape.

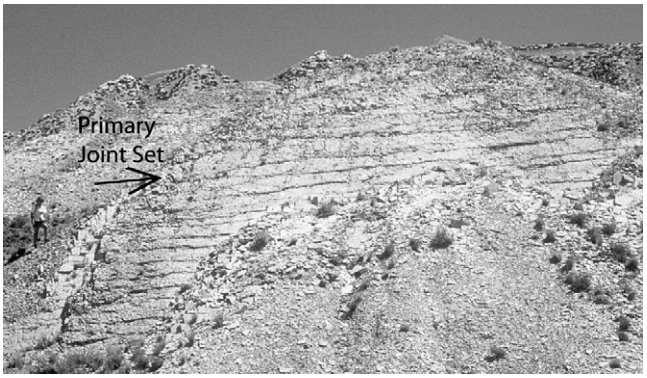

Fig. 3. Photos of typical outcrop in the Gypsum Springs formation. Black arrow points to primary fracture set.

To evaluate whether the earliest formed joints at the northern nose of Sheep Mountain Anticline predate folding, beds were rotated to horizontal with their associated joints (Fig. 4). Poles to joints after unfolding lie near the periphery of the stereonet (shallow plunges) with trends ranging from 0° to 360°. Because most sample sites fall on one of the two limbs of the fold, there are many points with similar orientation that can give the appearance of clusters. However, if the joints predate folding we would not see the range of joint trends observed in Fig. 4. The lack of strong joint clusters supports the interpretation that these joints developed during folding. In addition, the vast majority of the joints are perpendicular to bedding ($81° \pm 9°$), as expected for joints formed by flexure. Other processes, such as layer parallel shortening, can result in joint perpendicular to bedding, however such joints would have significant clustering of orientations. Recent studies by Bellahsen et al. (2006a) found semi-continuous early joint sets with similar strikes to other regional studies of pre-existing fracture sets (Allison, 1983; Garfield et al., 1992; Wicks et al., 2000). However, these joint sets are found in limited structural positions, i.e. the oldest set is found primarily along the limbs (and is similar to the

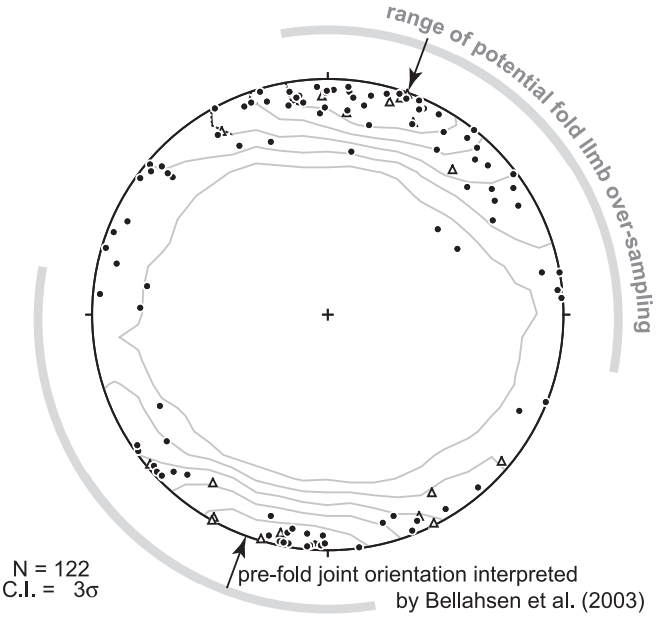

Fig. 4. Equal area steronet of orientation of primary joints after unfolding of beds about bed strike within the Gypsum Springs (triangles) and Sundance (circles) Formations at the northern nose of Sheep Mountain Anticline. Symbols are poles to joint planes. Kamb contour interval is three standard deviations from a uniform distribution.

orientations we measured along the limbs) and the second oldest set is absent in the forelimb. We would expect that fracture sets that predate folding should be present on all parts of the fold. The presence of prefold joints on the fold hinges is critical to demonstrating the interpretation, since joint orientations can be oversampled on the long limbs of plunging folds. Additionally, subsequent studies in the Phosphoria Formation found no prefolding joint set (Allwardt et al., 2007).

We find that the early joint pattern in each unit falls generally into one of two categories (Fig. 2C). We have colored the joint strikes so that all of the joints in a single unit have one color (red or blue) that corresponds to the overall pattern for that unit, even if some joints within that unit do not follow the pattern. Most units show a radial joint pattern along the southwestern limb where joints typically strike counter clockwise from bed strike (beds with red joints). This pattern is similar to the fracture pattern expected from present day fold curvature along the top of the bed (Fig. 1B). In contrast, most of the joints noted in blue on Fig. 2C strike clockwise from bed strike (e.g., Fig. 1E). We calculate the difference in strike between bedding and joints for each unit, using a positive angle to denote a counter clockwise difference from bed strike to joint strike (Fig. 5). The blue joints have a mostly negative (clockwise) difference in strike whereas red joints mostly strike counter clockwise from bed strike. The beds are in approximately the same structural position, thus we expect the stress field to have been similar if these beds fractured at the same time. Fig. 6 demonstrates this observation, showing two adjacent beds with primary joint sets at very different orientations. We postulate that the difference in observed joint patterns is due to the blue joints on Figs. 2 and 5 initiating earlier in the fold growth history when their host layers were in a different structural position. This hypothesis is supported by rock property testing that demonstrates these layers have a lower resistance to fracturing than the beds containing the red joints.

2.2. Rock property testing

In order to determine the relative timing of fracture in each bed, we tested rock properties in the field and in the laboratory on samples collected from six beds at the northern nose of Sheep Mountain Anticline. Laboratory tests of field samples for density and tensile strength provide quantitative values for assessing the fracture potential of each of the eight competent beds considered in this study. Sundance 1–5 beds are all fine- to medium-grained sandstones whereas Sundance 6 and 7, as well as Gypsum Springs are carbonates (Fig. 7). Unfortunately, available samples of the Sundance 3 and 4 beds were not suitable for testing. To determine the properties of these beds, we consequently rely on *in situ* testing and comparison to proxy beds of similar strength and lithology through hand sample investigation. Measurements of *in situ* stiffness of stratigraphic units, using a Schmidt hammer, can be used to correlate the relative strength of beds. The Schmidt hammer is a portable device that measures the rebound of a hammer impacting the rock (e.g. Poole and Farmer, 1980; Shackleton et al., 2005). The error in the stiffness values obtained from the Schmidt hammer can be evaluated from the range in multiple readings at the same locality (Poole and Farmer, 1980). Rebound values are corrected for the angle of the device during testing. For all tested competent beds, the average rebound values range from 50 to 58 (Table 1). These results suggest that the Sundance 3 and 4 beds have similar material properties as Sundance 2 beds. Furthermore, the rebound hammer results suggest that the Young's modulus does not vary significantly for these sedimentary units. This interpretation is supported by the measurement of similar dry unit weights for all the sampled beds (Table 2).

For the laboratory strength tests, cylindrical samples 2.54 cm in diameter and between 5.08 and 6.35 cm long were drilled from the samples so that the core axis is perpendicular to bedding. Cylinders were chosen to avoid weathered and fractured portions of the samples. The specimens were dried to remove excess water introduced by drilling. The samples were loaded at rates of approximately 0.5 KN/sec so that the compressive failure occurs after about 1 min of loading.

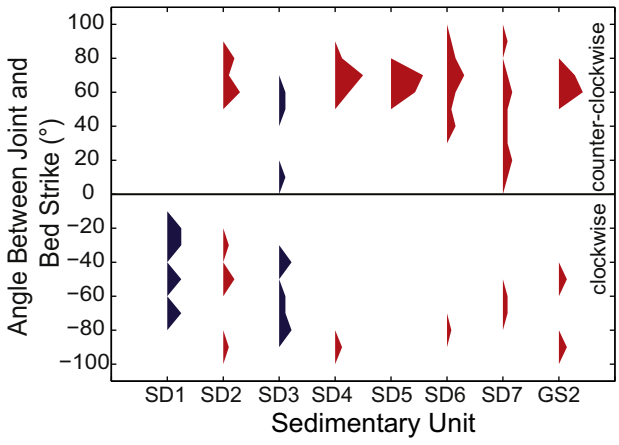

Fig. 5. Normalized histograms of difference in joint orientation from fold strike. Units labeled SD are from the Sundance Formation, unit labeled GS is from the Gypsum Springs Formation. A (counter) clockwise rotation in joint strike from bed strike is (negative) positive. The blue joints have a mostly negative rotation whereas the red joints are mostly positive.

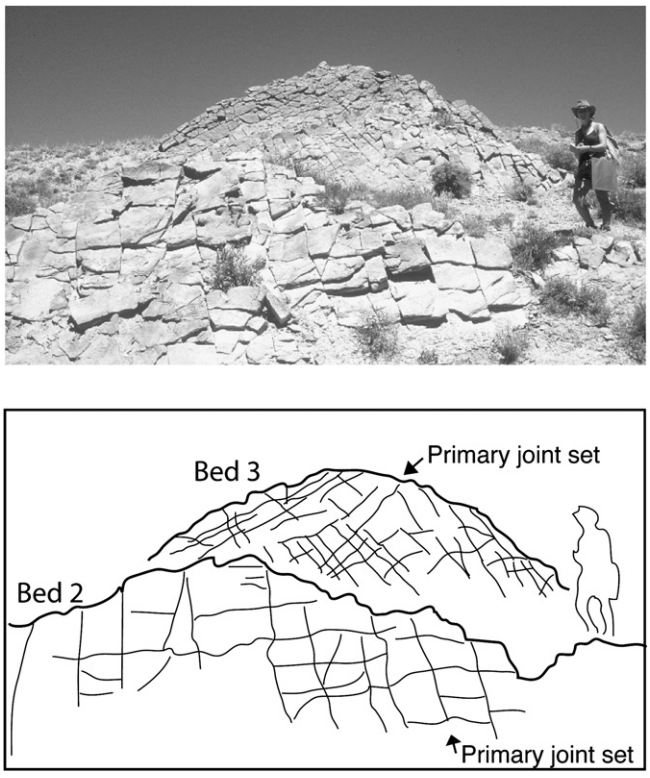

Fig. 6. Photograph and sketch of Beds 2 & 3 within the Sundance Formation with shale layer in between (person is standing on shale layer). Outcrop is located in the backlimb near the fold nose. Despite the proximity of the fractured beds, they have distinctly different joint orientations.

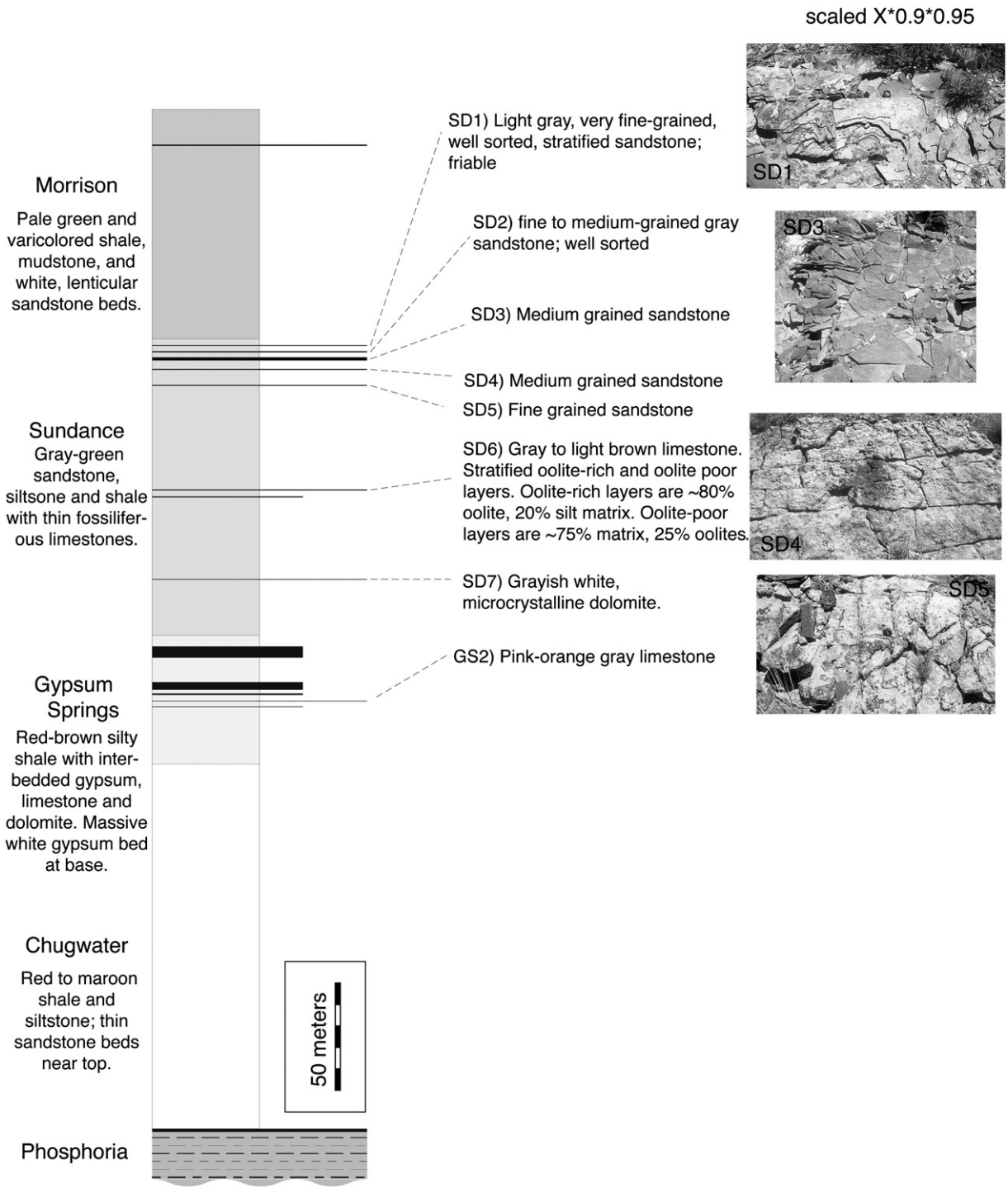

Fig. 7. Stratigraphic column of field area. Beds within the Sundance and Gypsum Springs Formations that are pertinent to this study are labeled. Note the visual difference in lithology between SD1 and SD3 compared to SD4 and SD5. Outcrop photos are located on the backlimb of the fold. Formation descriptions are modified from Rioux (1994).

The tensile strength of sampled mechanical units was directly assessed using the Brazilian laboratory test method. Cylinders 2.54 cm in diameter and at least 2.54 cm long are placed on their sides and subjected to compression across their diameters (ASTM, 1993). This compression induces tensile stresses at the points of load contact so that the peak compression at tensile failure can be converted to a tensile strength for the material (ASTM C496-90, Jaeger et al., 2007). At least 5 samples of each mechanical unit were tested and the average and standard deviation of tensile strength were determined (Table 2). Because existing cracks within the samples can reduce the measured tensile strength, we discard anomalous low strength values from the calculation of average tensile strength. The tensile strength varied from 3.3 ± 0.9 MPa in the Sundance 1 unit to 10.5 ± 1.8 MPa in the Sundance 5 unit (Table 1). Tensile strength for the Sundance 3 and 4 beds, which were not tested, were taken as average of Sundance 1 and 2 beds based on lithology and similar strength properties as determined by the Schmitt hammer tests.

Table 1

Unit	Bed Thickness (m)	Thickness Error	Tensile Strength (MPa)	Tensile Strength Error	Average Schmidt Rebound
SD1	0.24	0.08	3.3	0.9	–
SD2	0.44	0.41	6.9	1.5	53
SD3	1.2	0.59	5	1.0	52
SD4	0.35	0.21	5	1.0	56
SD5	0.35	0.18	10.5	1.8	–
SD6	0.35	0.29	2.4	0.6	58
SD7	0.19	0.09	7.1	2.0	–
GS2	0.18	0.14	6.3	1.3	50

Bed thickness measurements and tensile strength used to calculate fracture resistance for each bed. Bed thickness and tensile strength errors are one standard deviation from the mean.

2.3. Calculating fracture resistance of beds

Fracture resistance is the critical fold curvature required to develop joints (Eq. (3)). The fracture resistance depends on bed thickness, rock tensile strength and elastic properties. Considering that Poisson's ratio and Young's Modulus do not vary much for sandstone (e.g. Birch, 1966), the fracture resistance, F_r, simplifies to:

$$F_r = \frac{2T}{H} \tag{4}$$

Although present day strength of layers may not reflect the strength at the time of folding (e.g. Laubach et al., 2009; Shackleton et al., 2005), these sandstone beds should have experienced similar burial and diagenetic histories so that relative strength is consistent. Careful measurements of bed thickness were made in several locations for each unit. Fig. 8 shows the fracture resistance for each unit in our study. The variation in fracture resistance owes more to large bed thickness variability than variations in tensile strength (Table 1). Sundance 1 and 3 (blue beds in Figs. 2 and 5) have low resistance to fracture in the majority of the outcrops measured, whereas most of the other units have higher or more variable fracture resistance. This supports our postulate that Sundance 1 and 3 may have fractured earlier than the other beds in response to a different fold shape. The beds that show the most variation in fracture resistance (spanning the early–late fracture threshold) should show some scatter in the joint orientation. Now that a mechanical hypothesis for a discrepancy in fracture timing has been established, we predict a paleo-structural position to explain the early joint pattern seen at Sheep Mountain.

3. Joint prediction using plate bending theory and mechanical stratigraphy

Plate bending analysis considers the displacement and stress fields associated with folding of isolated mechanical units. Soft layers, such as the shales present at Sheep Mountain, compartmentalize deformation so that each more competent layer deforms as if isolated (e.g. Shackleton and Cooke, 2007), and we can model a relatively simple case of a laterally propagating fold (e.g. Delcaillau et al., 1998; Keller et al., 1999; Guillaume et al., 2008).

We approximate the shape of an anticline that may represent the early stage of folding at Sheep Mountain using a hybrid cosine-hyperbolic tangent function (Fig. 9);

$$f(x,z) = a\left(\tan h\left(\frac{x^2}{l^2}\right)\ \cos\left(\frac{\pi y}{d}\right)\right) \tag{5}$$

where a, l, and d are amplitude, length and width of the fold respectively (elevation drops from maximum at $(2l,0)$ to base elevation, or zero, at $(z = \pm d/2)$,. This function mimics the general

Table 2
Results of Laboratory Testing.

	Dry Unit Weight (Kn/m^3)	Tensile Strength (MPa)
Sundance 1		
1SD-1	23.78	
1SD-2		
1SD-3	23.38	
1SD-4		
1SD-5	23.27	
1SD-6	22.99	
1SD-7		2.7
1SD-8	23.54	3.9
1SD-9	25.96	4.8
1SD-10		2.9
1SD-11	23.96	2.5
1SD-13	23.80	3.0
Average	*23.83*	*3.31*
st. dev.	*0.92*	*0.87*
Sundance 2		
2SD-1		4.5
2SD-2		
2SD-3		
2SD-4	22.94	6.2
2SD-5	23.68	8.2
2SD-6		8.3
2SD-7	23.64	
2SD-8	24.16	6.5
2SD-9	24.13	5.4
2SD-10	24.76	9.6
2SD-11		
2SD-12		7.0
2SD-13	27.40	6.3
2SD-14	29.04	6.8
Average	*24.97*	*6.87*
st. dev.	*2.12*	*1.49*
Sundance 5		
5SD-1		
5SD-2	24.24	12.0
5SD-3		7.2
5SD-4		11.8
5SD-5	24.26	11.4
5SD-6		9.6
5SD-9	24.96	
5SD-10	25.27	
5SD-11	25.34	10.8
Average	*24.81*	*10.46*
st. dev.	*0.54*	*1.83*
Sundance 6		
6SD-1	22.23	
6SD-2	22.83	
6SD-3	24.46	
6SD-4	24.09	
6SD-5		1.8
6SD-6		2.0
6SD-7		2.8
6SD-8		2.0
6SD-9		2.4
6SD-10		3.5
6SD-11	25.74	
Average	*23.89*	*2.40*
st. dev.	1.35	0.64
Sundance 7		
7SD-1		
7SD-2	24.87	
7SD-3		
7SD-4		
7SD-5	25.20	
7SD-6	25.61	
7SD-7	26.51	8.5
7SD-8	25.28	5.6
7SD-9	25.72	8.6
7SD-10	24.94	8.5
7SD-11	22.03	4.4
Average	*25.02*	*7.13*
st. dev.	*1.32*	*1.96*
Gypsum Springs		

Table 2 (*continued*)

	Dry Unit Weight (Kn/m^3)	Tensile Strength (MPa)
GS-1	24.69	6.5
GS-2	25.00	6.5
GS-3		
GS-4		
GS-5		6.8
GS-6		
GS-7	24.69	5.8
GS-9		5.9
GS-10	25.45	
Average	*24.96*	*6.29*
st. dev.	*0.36*	*0.43*

shape of the plunging termination of an anticline flanked by synclines. Using a synthetic fold reduces noise by removing any small curvature deviations that do not correlate with fracture orientation (Allwardt et al., 2007). Additionally, present day curvature of Sheep Mountain most likely does not reflect the shape of the fold when joints formed, as 0.5–1 m thick beds can fracture when bed curvature is as small as 10^{-3}–10^{-4} m^{-1} (Eq (1)). Offsetting the function in Equation (5) in the x direction simulates stages in lateral along-axis fold propagation. We use this surface to represent the neutral surface of the fold, and compute joint patterns at the top and bottom of the beds.

Fig. 9A and B show predicted joint orientations for the top and bottom of a bed during an early stage of fold growth when folding is very gentle, and before the anticline has propagated along the strike of its axial surface. The joint trends in Fig. 9 represent the strike of bed-perpendicular joints, once the bed has been rotated to horizontal. Joint orientation predictions along the top of the bed are radial around the fold closure, whereas joint orientation predictions for the bottom of the bed strike 90° from the joints on the top of the bed. Because stresses are usually more tensile either on the top or bottom of the bed, one of these patterns will become the prevailing pattern for the whole bed. We further calculate whether two beds with different thicknesses and the same tensile strength will fracture due to the imposed folding. We use bed thicknesses of 0.2 and 1.2 m to reflect the range of thicknesses in our field area. The fracture resistance of these units would be 100 and 17 m^{-1} for the thinnest and thickest beds, respectively. These values of fracture resistance fall on either side of our proposed fracture resistance threshold between early and late episodes of fold growth

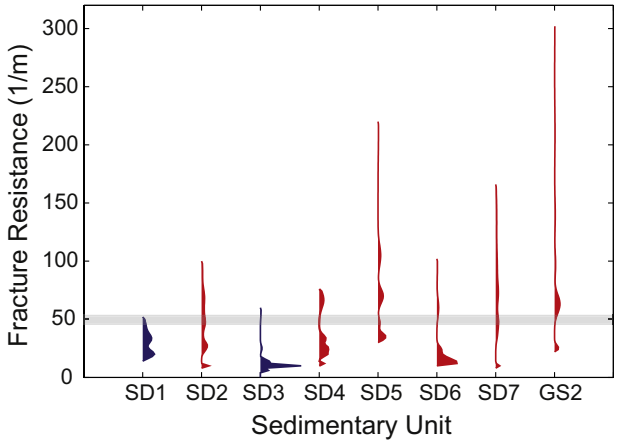

Fig. 8. Normalized probability distribution functions, plotted within the 95% confidence interval, of fracture resistance calculated from Equation (2) for each unit in the study. Bed units are labeled as in Fig. 4. Bed thickness was measured at almost every outcrop where fracture orientation was measured, and the spread of values mostly represents bed thickness changes along strike. The light gray bar approximates the resistance threshold between the beds with radial and non-radial fracture patterns.

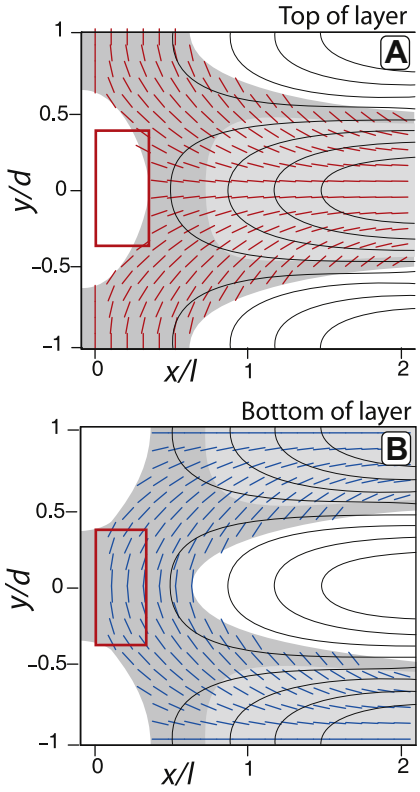

Fig. 9. Predicted joint patterns during early stage of fold growth. Upper plot (A) shows the strike of joints (red ticks) predicted to form due to outer arc tension on the top of each bed. Lower plot (B) shows the strike of joints (blue ticks) predicted to form due to outer arc tension of the adjacent synclinal areas on the bottom of each bed. Contours show shape of the fold, contour interval is 2 m. Light gray shading denotes a zone where stresses in a 0.2 m thick bed would exceed an effective tensile strength of 10 MPa. Dark gray shading denotes a zone where stresses in a 1.2 m thick bed would exceed an effective tensile strength of 10 MPa. Thicknesses of 0.2 and 1.2 m reflect the thinnest and thickest units studied.

(Fig. 8). Areas where only less resistant beds will fracture (effective tension on outer surface >10 MPa) are shown in dark gray and areas where both beds will fracture are light gray. The white sections represent areas that will not fracture (stresses on both beds <10 MPa). For the structural position we are interested in (the fold termination and the area directly in front of the early fold closure), the fracture pattern will reflect the stresses along the top of the bed. One exception is in front of the fold nose where the top of the bed will not fracture (red box Fig. 9). The stresses along the bottom of a bed in this area exceed the tensile strength only of the less resistant beds (dark gray) because curvatures of this concave upward section of the fold are small. As the fold grows laterally along its axis, formations that were located in front of the inflection line will lie in a new structural position behind the inflection line. Such folds may contain some less resistant beds that fractured from the bottom surface of the bed early in folding and other more resistant beds that fractured from the top surface of the bed later in folding. In this case, their joints will strike 90° from one another.

4. Interpretation and discussion of joints on folds

Our field data from the nose of Sheep Mountain Anticline show similarities to the predicted joint patterns. Joints in the more fracture resistant strata show a generally radial pattern, similar to the pattern produced by stresses on the top of the fold. Joints in the two less resistant beds of the anticline strike orthogonally from the radial pattern and resemble the predicted pattern for bottom-initiated

joints (Fig. 2). We interpret this to indicate that the fractures in these two units formed when the tensile stresses at the bottom of the plate were greater than the top, meaning these beds must have been ahead of the inflection line in the area where the fold was concave upwards at the time of fracturing. Because this area is now behind the inflection line (Bellahsen et al., 2006a), Sheep Mountain Anticline and its underlying fault may have grown laterally along the fold axis between the two fracture episodes (e.g. Fig. 1F). The interpretation of the data in this way represents a new method of identifying fold and underlying fault growth. Here we only document two joint categories (early and late) but in folds where beds have more widely varying fracture resistance, multiple fracture generations may be deduced. Previous studies at Sheep Mountain have deduced that there was no lateral fold growth, based on the variation in early joint orientations at the northern nose being interpreted as fault tip related (Bellahsen et al., 2006a). However, if there was no prefolding fracture set (as we found in our study here), this variation in joint orientation could also be related to fold nose curvature.

The observation that joints may initiate from stresses at the bottom of the beds as well as the top is novel, and may help elucidate joint patterns on other folds. In future studies, this idea can be further explored by documenting joint surface morphology. Plumose patterns on joint faces reveal the joint propagation direction (Pollard and Aydin, 1988) and we can confirm if patterns reflecting stresses on the bottom of the layer indeed propagated from the bottom.

The plate bending models in Fig. 9 represent a simple case of gently folded, axially symmetric layers. Localized folding and faulting (such as the small fault cutting across SMA in Fig. 2), fault tip stresses, bed contact friction, and the tightly folded adjacent syncline are some of the factors that may perturb the local stress field and influence joint trends at Sheep Mountain. Thus, we expect natural joints sets to have some inherent variability, such as we see on the northeast side of the fold.

5. Conclusions

We demonstrate that differences in joint pattern between beds in the same structural position at Sheep Mountain Anticline may reflect lateral fold propagation over time. The beds with joint patterns that are inconsistent with present day fold curvature also have less fracture resistance than beds that have joints that match predictions from present day curvature. Plate bending theory predicts that joints initiate from the outer arc of the folded bed and that joint patterns resulting from stresses on the top and bottom of a bed will be 90° from one another, which approximates the difference in joint strikes between early and late fractured beds at Sheep Mountain. Ahead of the inflection line on the nose profile, joints will initiate from the bottom of the layer, whereas behind the inflection line, joints initiate from the top of the layer. However, only the least resistant beds fracture in front of the inflection line due to low curvatures. After a fold has propagated laterally along its axis, beds that fracture early in the fold history show fracture patterns that are inconsistent with the stresses that would be predicted from curvature analysis of their present structural position.

Acknowledgements

We would like to thank Erika Davis and Rain Nourne for field assistance at Sheep Mountain. This paper has been greatly improved by reviews from Mark Fischer and Nicolas Bellahsen. We would also like to thank our associate editor, Tom Blenkinsop, as well as Christie Rowe and Jamie Kirkpatrick for reading early drafts of the paper.

References

Allison, M.L., 1983. Deformation styles along the Tensleep fault, Bighorn Basin, Wyoming. In: Wyoming Geological Association Guidebook, 34th Annual Field Conference.

Allwardt, P.F., Bellahsen, N., Pollard, D.D., 2007. Curvature and fracturing based on global positioning system data collected at Sheep Mountain Anticline, Wyoming. Geosphere 3 (6), 408–421. doi:10.1130/GES00088.1.

Amrouch, K., Lacombe, O., Bellahsen, N., Daniel, J.M., Callot, J.-P., 2010. Stress and strain patterns, kinematics and deformation mechanisms in a basement-cored anticline: Sheep Mountain Anticline, Wyoming. Tectonics 29, TC1005. doi:10.1029/2009TC002525.

ASTM, 1993. Standard test method for splitting tensile strength of cylindrical concrete specimens (C496-90). In: 1993 Annual Book of ASTM Standards, Sect. 4, Vol. 04.02. ASTM, Philadelphia, PA, pp. 269–272.

Bellahsen, N., Fiore, P., Pollard, D.D., 2006a. The role of fractures in the structural interpretation of Sheep Mountain Anticline, Wyoming. Journal of Structural Geology 28 (5), 850–867.

Bellahsen, N., Fiore, P.E., Pollard, D.D., 2006b. From spatial variation of fracture patterns to fold kinematics; a geomechanical approach. Geophysical Research Letters 33, L02301. doi:10.1029/2005GL024189.

Birch, F., 1966. Compressibility: elastic constants. In: Clark Jr., S.P. (Ed.), Handbook of Physical Constants. Geological Society of America, pp. 97–174.

Cruikshank, K., Zhao, G., Johnson, A., 1991. Analysis of minor fractures associated with joints and faulted joints. Journal of Structural Geology 13 (8), 865–886.

Delcaillau, B., Deffontaines, B., Floissac, L., Angelier, J., Deramond, J., Souquet, P., Chu, H.T., Lee, J.F., 1998. Morphotectonic evidence from lateral propagation of an active frontal fold; Pakuashan Anticline, foothills of Taiwan. Geomorphology 24 (4), 263–290.

Engelder, T., Gross, M.R., Pinkerton, P., 1997. Joint development in clastic rocks of the Elk Basin anticline, Montana-Wyoming. In: Hoak, T., Klawitter, A., Blomquist, P. (Eds.), Fractured Reservoirs: Characterization and Modeling: Rocky Mountain Association of Geologists 1997 Guidebook, pp. 1–18. Denver, Colorado.

Fischer, M.P., Wilkerson, M.S., 2000. Predicting the orientation of joints from fold shape; results of pseudo-three-dimensional modeling and curvature analysis. Geology 28 (1), 15–18.

Forster, A., Irmen, A.P., Vondra, C., 1996. Structural interpretation of Sheep Mountain Anticline, Bighorn Basin, Wyoming. Wyoming Geological Association Guidebook 47, 239–251.

Garfield, T.R., Hurley, N.F., Budd, D.A., 1992. Little Sand Draw Field, Big Horn Basin, Wyoming: a hybrid dual-porosity and single-porosity reservoir in the phosphoria formation. AAPG Bulletin 76, 371–391.

Green, G.N., Drouillard, P.H., 1994. The Digital Geologic Map of Wyoming in ARC/INFO Format, 1:500000. United States Geological Survey, Denver, CO.

Guillaume, B., Dhont, D., Brusset, S., 2008. Three-dimensional geologic imaging and tectonic control on stratigraphic architecture: upper cretaceous of the Tremp Basin (south-central Pyrenees, Spain). AAPG Bulletin 92 (2), 249–269.

Harris, J.F., Taylor, G.L., Walper, J.L., 1960. Relation of deformational fractures in sedimentary rocks to regional and local structures. Bulletin of the American Association of Petroleum Geologists 44 (12), 1853–1873.

Hennier, J., Spang, J.H., 1983. Mechanisms for deformation of sedimentary strata at Sheep Mountain anticline, Bighorn Basin, Wyoming. In: Wyoming Geological Association Guidebook, 34th annual field conference, pp. 97–111.

Hennings, P.H., Olson, J.E., Thompson, L.B., 2000. Combining outcrop data and three-dimensional structural models to characterize fractured reservoirs; an example from Wyoming. AAPG Bulletin 84 (6), 830–849.

Jackson, J., Norris, R., Youngson, J., 1996. The structural evolution of active fault and fold systems in central Otago, New Zealand: evidence revealed by drainage patterns. Journal of Structural Geology 18 (2–3), 217–234.

Jaeger, J.C., Cook, N.G.W., Zimmerman, R.W., 2007. Fundamentals of Rock Mechanics. Blackwell Publishing, Malden, MA.

Johnson, J.D., Garside, L.G., Warner, A.J., 1968. A study of the structure and associated features of Sheep Mountain anticline, Bighorn County, Wyoming. Earth Science Bulletin 1, 25–28.

Keller, E.A., Gurrola, L., Tierney, T.E., 1999. Geomorphic criteria to determine direction of lateral propagation of reverse faulting and folding. Geology 27 (6), 515–518.

Laubach, S.E., Olson, J.E., Gross, M.R., 2009. Mechanical and fracture stratigraphy. AAPG Bulletin 93 (11), 1413–1426.

Nelson, R.A., 1985. Geological Analysis of Naturally Fractured Reservoirs. Gulf Publishing Company, Houston, Texas.

Pavlis, T.L., Bruhn, R.L., 1988. Stress history during propagation of a lateral fold-tip and implications for the mechanics of fold-thrust belts. Tectonophysics 145, 1–2.

Pollard, D.D., Aydin, A., 1988. Progress in understanding jointing over the past century. Geological Society of America Bulletin 100, 1181–1204.

Poole, R.W., Farmer, L.W., 1980. Technical note: consistency and repeatability of Schmidt hammer rebound data during field testing. International Journal of Rock Mechanics and Mining Sciences and Geomechanics Abstracts 17, 167–171.

Price, N.J., Cosgrove, J.W., 1990. Analysis of Geologic Structures. Cambridge University Press.

Rioux, Robert L., 1994. Geologic Map of the Sheep Mountain – Little Sheep Mountain Area, Bighorn County, Wyoming. Open-File Report 94-191, U.S. Geological Survey.

Roering, J.J., Cooke, M.L., Pollard, D.D., 1997. Why blind thrust faults do not propagate to the Earth's surface: numerical modeling of coseismic deformation associated with thrust-related anticlines. Journal of Geophysical Research – Solid Earth 102 (B6), 11901–11912.

Savage, H.M., Cooke, M.L., 2004. The effect of non-parallel thrust fault interaction on fold shape. Journal of Structural Geology 26, 905–917.

Scholz, C.H., 2002. The Mechanics of Earthquakes and Faulting. Cambridge University Press.

Shackleton, J.R., Cooke, M.L., Sussman, A.J., 2005. Evidence for temporally changing mechanical stratigraphy and effects on joint network architecture. Geology 33, 101–104.

Shackleton, J.R., Cooke, M.L., 2007. Is plane strain a valid assumption for non-cylindrical folds? Journal of Structural Geology 29, 1229–1240.

Stanton, H.I., Erslev, E.A., 2004. Sheep Mountain Anticline: backlimb tightening and sequential deformation in the Bighorn Basin, Wyoming. Wyoming Geological Association Guidebook 53, 75–87.

Stein, R.S., King, G.C., 1984. Seismic potential revealed by surface folding:1983 Coalinga, California, earthquake. Science 224 (4651), 869–872. doi:10.1126/science.224.4651.869.

Turcotte, D.L., Schubert, G., 2002. Geodynamics. Cambridge University Press.

Wicks, J.L., Dean, S.L., Kulander, B.R., 2000. Regional tectonics and fracture patterns in the Fall River formation (Lower Cretaceous) around the Black Hills foreland uplifts, western South Dakota and northeastern Wyoming. In: Cosgrove, J.W., Ameen, M.S. (Eds.), Forced Folds and Fractures. Geological Society of London Special Publication 169, pp. 145–165.